Turkevych, I.; Ryukhtin, V.; Garamus, V.; Kato, S.; Takamasu, T.;
Kido, G.; Kondo, M.:

Studies of self-organization processes in nanoporous alumina membranes by small-angle neutron scattering

In: Nanotechnology (2012) IOP

DOI: 10.1088/0957-4484/23/32/325606

Studies of self-organization processes in nanoporous alumina membranes by small-angle neutron scattering

Ivan Turkevych[1*], Vasyl Ryukhtin[3], Vasyl Garamus[4], Seiichi Kato[2], Tadashi Takamasu[2], Giyuu Kido[2] and Michio Kondo[1]

[1]National Institute of Advanced Industrial Science and Technology, AIST Central 2, 1-1-1 Umezono, Tsukuba, Ibaraki, 305-8568, Japan

[2]National Institute for Materials Science, Sengen 1-19-2, Tsukuba, Ibaraki 305-0047, Japan

[3]Helmholtz-Zentrum Berlin for Materials and Energy, Department of Structural Research, Hahn-Meitner-Platz 1, 14109 Berlin, Germany

[4]Geesthacht Neutron Facility, GKSS Research Centre, Max-Planck-Str. 1, D-21502 Geesthacht, Germany

*E-mail: Ivan.Turkevych@aist.go.jp (corresponding author)

Abstract

We performed studies of the self-organization processes in nanoporous alumina membranes at initial and late stages of aluminium anodization by using scanning electron microscopy (SEM) and small-angle neutron scattering (SANS). SEM observations indicated three stages in the self-organization of nanopores in alumina: (1) nucleation of random nanopores with a broad radius distribution, (2) narrowing the radius distribution and (3) slow evolution of the nanoporous structure toward ordering of nanopores into large domains. SANS studies revealed orientational correlation between ordered domains of nanopores, which is characterized by a small misorientation angle. For the samples with high aspect ratio of nanopores, the SANS patterns showed azimuthal smearing, which was attributed to the redistribution of nanopores between the domains during their growth.

PACS: 61.46.-w, 82.45.Yz

1. Introduction

Aluminium anodization [1] is one of the most controllable self-organized processes yielding vertically aligned uniform cylindrical nanopores. These nanopores can be used as nano-beakers for either self-assembly or synthesis of nanomaterials. Nanoporous alumina (NPA) membranes have been used to fabricate a wide variety of diverse nanostructures such as quantum dots [2], nanowires [3, 4], carbon nanotubes [5], nanostructured films [6] and photonic structures [7]. The geometry of the nanoporous structure, such as interpore distance, pore diameter and length, can be varied in a wide range by adjusting conditions of aluminium anodization and post-anodizing treatment [8]. Besides vertical alignment, nanopores tend to form ordered hexagonal arrays under specific conditions [9]. Thus, laterally disordered as well as highly-ordered nanoporous alumina membranes can be fabricated.

The most important feature of the NPA is the high aspect ratio of nanopores, which creates an excellent opportunity for the fabrication of long and more importantly monodisperse nanowires inside the long pores [10]. However, the straightforward characterization of the thick NPA membranes by microscopic methods such as scanning electron microscopy (SEM) or atomic force microscopy (AFM) cannot provide information about their properties in a bulk. Due to the high penetration of neutrons, the small angle neutron scattering (SANS) is a technique of choice that enables non-destructive studies of nanostructured materials [11] and can provide viable information about their bulk structure, which is complimentary to the SEM analysis [12-15]. SANS signal originates from the whole sample and is delicate enough to sense volume fraction fluctuations at tenths of percent, which make SANS one of the preferable methods for the characterization of nanoporous materials. SANS is also efficient for studies of nano-scale ordering of hard- (i.e. nanoporous ceramic, semiconductor, metal) and soft- (i.e. co-polymer, liquid crystal, etc.) materials. The 2D SANS diffraction pattern can reveal size distribution and positional correlation of nanopores or nano-scale inclusions of secondary phases in the whole sample. The theoretical description of the neutron scattering from nanotubular systems has been addressed by Oster and Riley [16], who derived expressions for the intensity of neutron scattering by the media composed of infinitely long cylinders. Also, the effects related to the transition from random distribution of the parallel cylinders to their hexagonal ordering have been described.

Although experimental SANS studies on nanoporous alumina have been already reported [17-21], most of them were performed on samples with disordered porous structure. Also, to the best of our knowledge, there are no SANS studies that reveal dynamics of the self-organization processes in nanoporous alumina. In this paper small-angle neutron scattering (SANS) and scanning electron microscopy (SEM) studies have been used in a complementary manner, which enabled us to study self-organization of the nanoporous structure on different stages of the anodization process.

2. Experimental

The nanoporous alumina membranes were fabricated by anodization of 99.99% pure aluminium sheets. The aluminium substrates were first annealed at 500 °C in argon atmosphere and then electropolished in a mixture of perchloric acid and ethanol 1:4 to obtain a smooth mirror-like surface. The anodization of the electropolished aluminium was performed in a two-electrode cell with the aluminium sheet as anode and a platinum mesh as the counter electrode under the constant potential of 40V in 0.3M oxalic acid electrolyte at 5 °C. The electrolyte solution was vigorously stirred to improve the uniformity of the temperature distribution and to minimize diffusion limitations in long nanopores.

The ordering of the nanopores during initial stages of their growth was studied by interruption of the anodization process, selective dissolution of the anodic oxide layer in a mixture of chromic (20 g/l) and phosphoric (66 g/l) acids at 60 °C and SEM observation of structural features remained on the surface of aluminium, which replicates the morphology of the Al/Al_2O_3 interface (figure 1).

The highly ordered nanoporous alumina membranes were fabricated by using the two steps anodization technique described by Masuda [22]. The first anodization step lasted 18 hours to promote the ordering of nanopores. Then the thick nanoporous layer was selectively dissolved in the mixture of chromic and phosphoric acids leaving the highly-ordered concave patterns on the surface of aluminium. The ordered concaves acted as a self-assembled mask for the nucleation of pores during the second anodization step. The second anodization was performed under the same parameters, except different anodization times were used for the fabrication of membranes with desirable thicknesses. By using this technique, a set of highly-ordered nanoporous alumina membranes with the interpore distance of 100 nm, pore diameter of 30 nm and thickness of 15.5 μm, 40 μm and 55 μm was fabricated. Then the diameter of nanopores was increased to 50 nm by isotropic etching in 5% phosphoric acid at room temperature. In addition, the last sample of the above mentioned set with the thickness of 55 μm was divided into two pieces and the diameter of nanopores in one piece was widened to 75 nm in order to probe the dependence of the SANS signal intensity on the diameter of nanopores. The aluminium remained on the back side of the membranes was selectively dissolved in the saturated $HgCl_2$ solution at room temperature. All samples were carefully cleaned in distilled water to remove the traces of chemicals used during their fabrication and then observed in field-emission scanning electron microscope (FE-SEM, JEOL 6500F).

Neutron scattering experiments were performed on the SANS-1 instrument at the GKSS research centre (Geesthacht, Germany). The schematic setup of the pin-hole SANS is shown in figure 2(a). The variation of the distance *SD* between the sample and the 2D position sensitive detector enabled us to adjust resolution of the instrument, because scattering vector Q is related to the geometry of the instrument as $Q = (4\pi/\lambda)\sin(\Theta/2) = (4\pi/\lambda)\sin(0.5\arctan(X/SD))$, where λ is the neutron wavelength. The measurements were performed at different sample-detector distances (*SD*) of 0.7, 1.8, 4.5 and 9.97 m in order to cover the *Q*-range continuously from 5×10^{-3} Å^{-1} to 0.25 Å^{-1}. The distance of 9.97 m gave the best resolution, which was close to the largest possible SD distance of our SANS instrument. At this distance the first order reflections were nicely detectible and the reflections of second order can be resolved. At closer distances only Porod's scattering was measured because of high instrumental smearing. The neutron wavelength used in the experiment was 8.19 Å with $\Delta\lambda/\lambda=0.1$. The beam size at the sample was 4 mm in diameter. The central part of the detector was shielded by a "beam-stop" in order to protect the detector against damage. The samples were installed perpendicularly to neutron beam with the axis of cylindrical pores parallel to the incident beam direction.

3. Results and discussion

The anodization of aluminium starts from the formation of a dense barrier oxide layer [1]. The maximal thickness of the barrier layer is given by the applied potential and pH of the electrolyte. As the barrier layer grows, the density of the anodization current decays exponentially as shown in the first section of the figure 1(e). In neutral electrolytes the anodization process stops at this stage, however in acidic ones continues in a porous growth regime. The nucleation and subsequent growth of nanopores elevates the current density back to a

certain value and then the current remains stable, which corresponds to the balance between oxide formation at the Al/Al_2O_3 interface and oxide dissolution at the Al_2O_3/electrolyte interface. The nucleation of nanopores occurs on structural flaws of the barrier oxide layer, which concentrate the electric field and promote field assisted dissolution of the oxide. The aluminium density is 3.2 g/cm^2 while the density of aluminium oxide is 2.8 g/cm^2 which results in volume expansion in the oxide layer and compressive stress on the Al/Al_2O_3 interface. The relaxation of the compressive stress is the main driving force that promotes formation and ordering of the nanopores [9, 10].

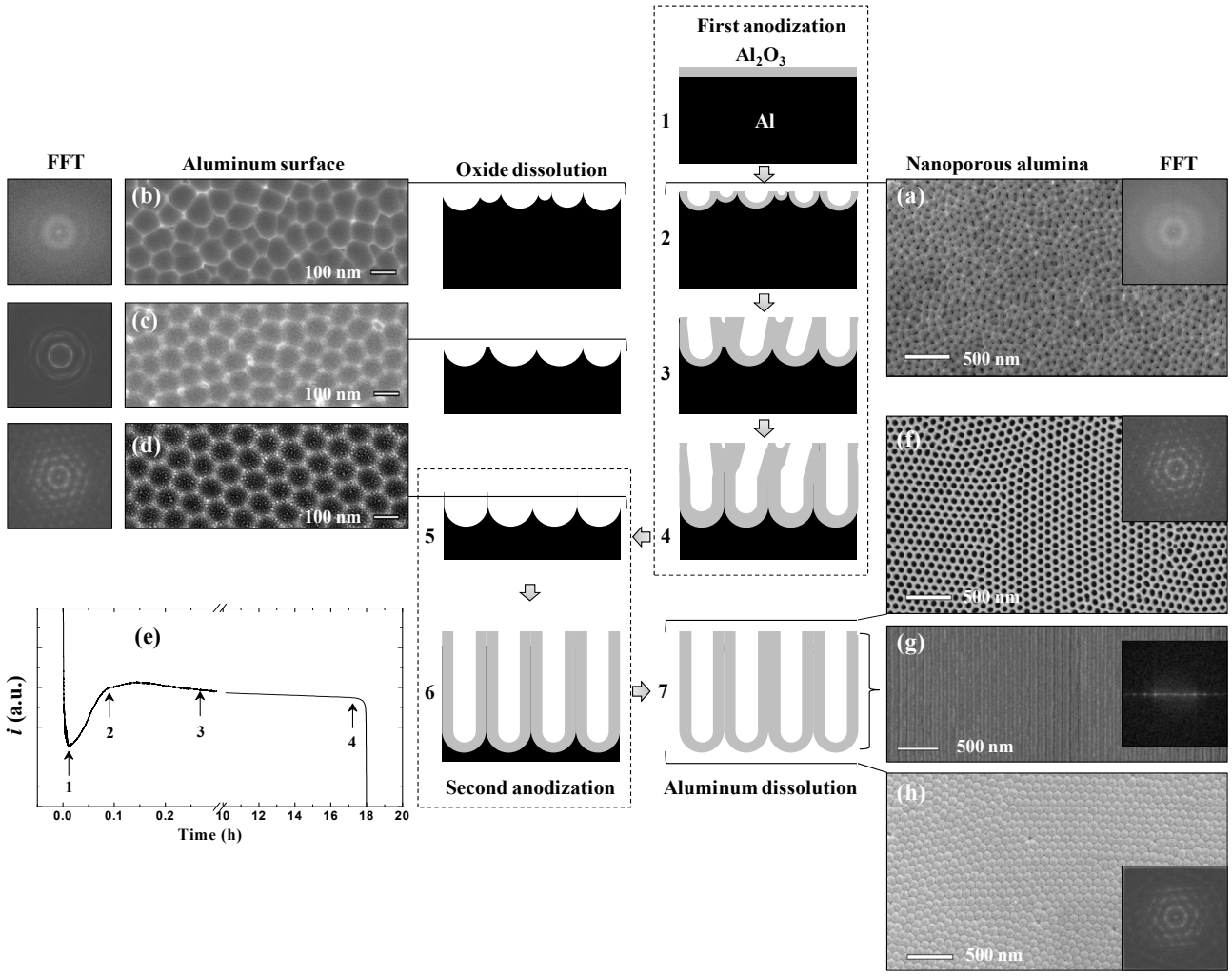

Figure 1. Schematic diagram illustrating the fabrication of nanoporous alumina (NPA) membranes by two steps anodization technique and SEM images showing stages of the self-organization process. (a) The SEM image of the disordered NPA after nucleation of nanopores. During the first anodization, the growth of the NPA was interrupted at points 2, 3 and 4 designated by arrows on current-time transient curve (e). The correspondent SEM images (b), (c) and (d) were taken after dissolution of the porous oxide layer. The second anodization started from the aluminium sample with ordered concaves and the top (f), side (g) and bottom (h) view SEM images were taken after the NPA reached the desirable thickness and the remained aluminium was dissolved. FFT patterns are shown as insets at the corresponded SEM images.

The SEM images shown in figures 1(b)-1(d) reveal that the stress relaxation at the Al/Al_2O_3 interface undergoes several stages. Immediately after the generation of pores in the barrier layer (figure 1(a)) the Al/Al_2O_3 interface acquires a random morphology of irregular polydisperse concaves shown in figure 1(b). The correspondent Fast Fourier Transform (FFT) pattern displays highly blurred circular ring which indicates absence of the spatial ordering as well as the broad radius distribution of the concaves. The radius distribution function of the concaves then becomes highly peaked. The central ring on the FTT pattern of figure 1(c) has six maxima, which are highly blurred in azimuthal direction. At this stage the Al/Al_2O_3 interface can be described as a disordered "liquid" of monodisperse concaves without long range ordering. Finally, the nanoporous system undergoes slow evolution toward hexagonal ordering of nanopores into large domains. The FFT pattern of the figure 1(d) displays six intense reflections typical for a two-dimensional hexagonal lattice. In addition, several higher order reflections are observed confirming the highly ordered hexagonal arrangement.

The second anodization starts from the formation of barrier layer on the aluminium surface, which already comprises ordered concaves. Therefore the field assisted dissolution of the oxide and nucleation of pores occurs over the concaves. Thus, the nanopores replicate the ordered nanoporous structure attained during the first long anodization step. After the completion of the second anodization, dissolution of the remained aluminium and some widening of pores, the stand alone nanoporous alumina membranes were inspected in SEM. The top, side and bottom SEM images with correspondent FFT patterns are shown on figures 1(f), 1(g) and 1(h) respectively. The nanopores are spatially organized into large ordered domains with some linear defects at the domain boundaries and few point defects, which exhibited as distorted pores that surround white protruding hills. Here, under defects we mean disorders in the ideal hexagonal arrangement of the nanoporous structure.

Although the degree of the ordering and the size of the domains look similar at the top and at the bottom side of the membranes, the SEM can picture only a small sample area and the FFT pattern can be derived only from several ordered domains, which does not allows estimation of the misorientation degree between domains in the whole sample. In addition, the SEM observation of the cross section cannot provide excessive information about porous structure in the bulk of the sample because only few cross-sections can be studied.

To overcome the limitations of the SEM technique and to reveal the structure of the nanoporous alumina membranes in the bulk, the 2D SANS patterns were measured for the set of membranes with different thickness. Whereas structures with randomly oriented domains must lead to the smearing of the SANS patterns similar to the powder diffraction scattering, the fully isotropic patterns were not observed in the case of highly-ordered nanoporous alumina membranes. The six-spot hexagonal pattern in figure 2(b) indicates that the nanoporous alumina membranes consist of hexagonally ordered domains, which have a preferential orientation over the sample area. To the best of our knowledge, the existence of such domain orientation has not been reported previously for nanoporous anodic alumina. In the case of ideal ordering, the pores would be arranged into a perfect hexagonal lattice, resulting in the SANS diffraction pattern that consists of sharp spots. Deviations from this ideal situation are manifested by broadening of the SANS spots in azimuthal and radial directions. The azimuthal broadening is due to the misorientation of the domains while the broadening in radial direction is due

the gradual loss of the positional correlations of interpore distances. The ordering degree is then characterized by the two full-width-at-half-maximum values taken from Gaussian fits of the intensity distributions of the diffraction spots in azimuthal and radial directions, known as "ϕ-mosaic" and "χ-mosaic", respectively.

We attribute the existence of this orientational correlation to the same compressive stress on the Al/Al_2O_3 interface that promotes hexagonal ordering of nanopores, because large misorientation angles between domains are not energetically favourable. The theoretical analysis on the motion of grain boundaries in hexagonal structures [23] demonstrates that the defects diffusion at the grain boundaries is affected by short range forces, which strongly depend on the misorientation angle between domains. As a result, the domain structure eventually reaches metastable quasi-crystalline configuration with a small misorientation angle between the domains.

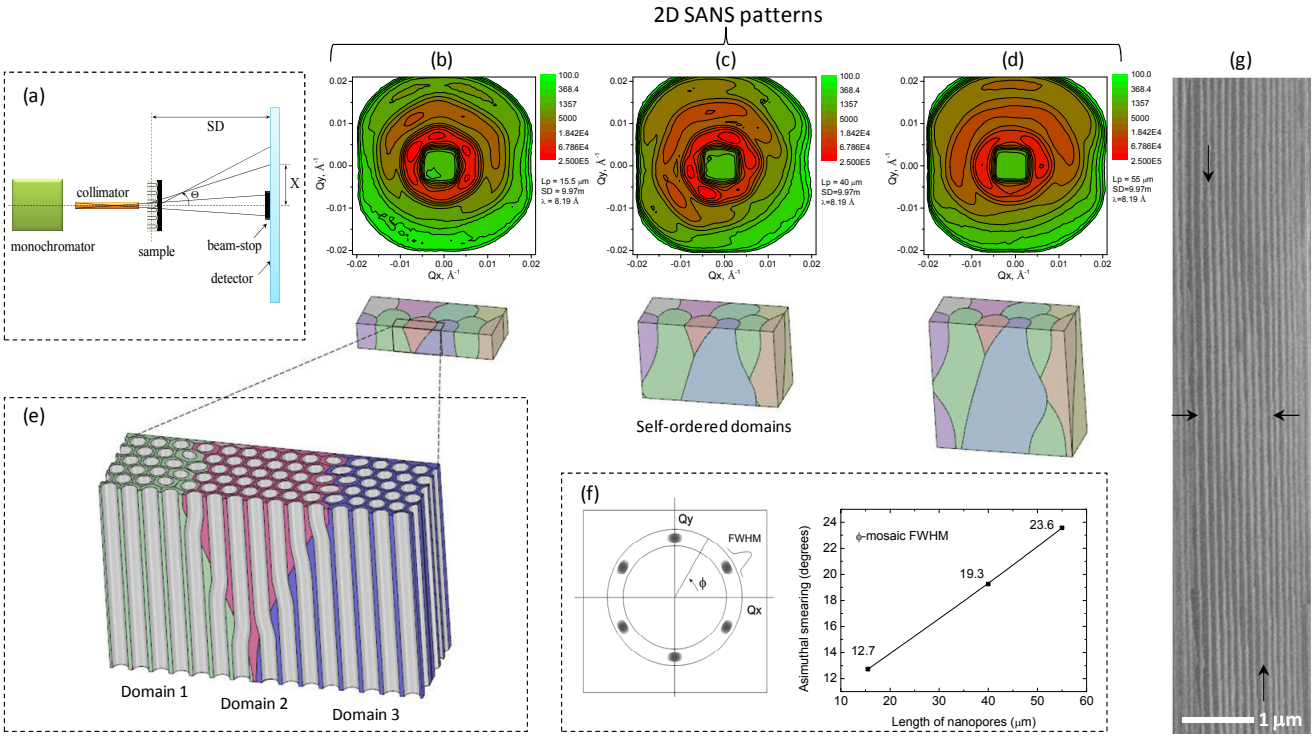

Figure 2. 2D SANS patterns measured on NPA samples with the thickness of (b) 15 μm, (c) 40 μm and (d) 55 μm at sample-detector distance of 9.97 m. The schematic illustrations below the SANS patterns shows portions of the NPA samples with self-ordered domains depicted in different colours (note that the scale is not kept). The zoomed inset (e) illustrate how nanopores migrate from one domain to another across grain boundaries upon elongation. The cross-section SEM image (g) shows the evolution of a typical domain, where arrows designate the point of the domain origin, its maximum width and the point of fade. The inset (f) shows the dependence of azimuthal smearing of the SANS pattern (ϕ-mosaic full-width-at-half-maximum FWHM) on the length of nanopores. The inset (a) shows the arrangement of our pin-hole SANS instrument.

The circular averages of SANS signal obtained from the nanoporous membranes samples with different diameter of nanopores (figure 3) permit determination of the mean interpore distance by the position of the main peak in Q-space by using simple equation: $d_{10}=2\pi/|Q|$, where $Q=(4\pi/\lambda)\times\sin\Phi/2$ is the momentum-transfer vector and Φ is the scattering angle. The positions of the first order peaks are clearly seen at $|Q_{10}|=0.0062$ Å^{-1}, which gives $d_{10}=101$ nm. This value is in good agreement with the interpore distance of 100 nm estimated from the SEM images. Secondary peaks are weaker, however, are detectible at $2*|Q_{10}|$ position. Third and further reflection are smeared by instrumental curve and cannot be detected on a background of the Porod's tail. The intensity of the scattering curves increases with the increasing of the diameter (d_p) of nanopores. The nanoporous alumina membranes give a very strong SANS signal even from very thin samples, which makes the nanoporous alumina an excellent etalon material for the calibration of SANS instruments.

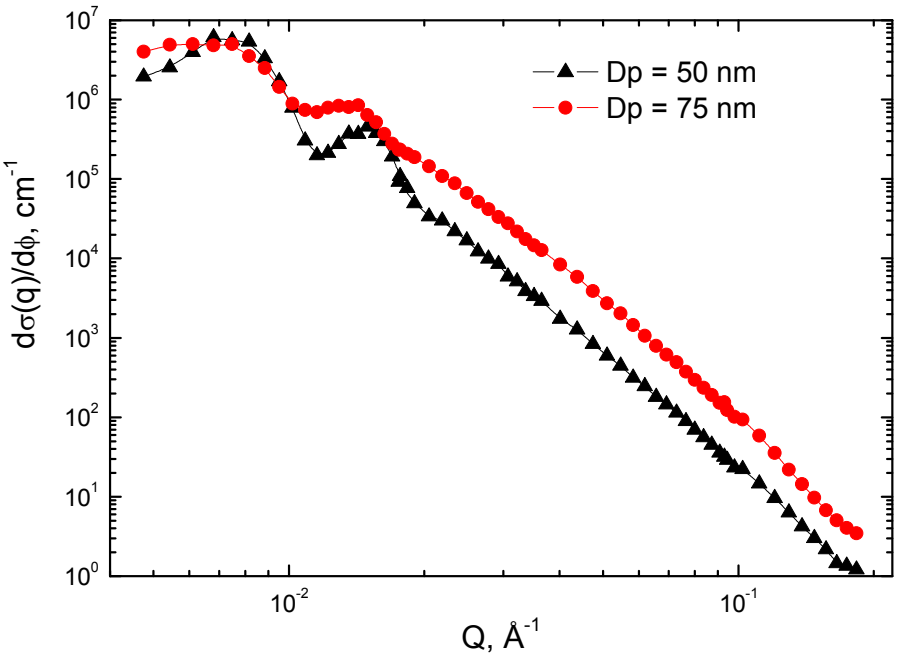

Figure 3. Circular averages of SANS patterns measured on NPA samples with interpore distance of 100 nm, thickness of 55 μm and different diameter of the nanopores: 50 nm (triangles) and 75 nm (circles).

The six-spot hexagonal pattern shown in figure 2(b) indicates that the cylindrical pores are parallel to the incident neutron beam. However the scattering patterns smear azimuthally with the increasing of the porous layer thickness (figures 2(c)-2(d)). SANS pattern measured from the thickest sample looks almost isotropic (figure 2(d)). However, the level of smearing in the radial direction remains the same, which means that the average distance between nanopores is constant in the bulk of the material. The azimuthal smearing of the SANS pattern can be attributed to the twisting of nanopores, which transit from one domain to another across domain boundaries during their growth. The redistribution of individual nanopores across the domain boundaries dynamically affects both the shape and the size of the individual domains. Although all nanopores pass the entire

membrane from top to bottom (i.e. there is no renucleation of nanopores in the bulk of the membrane), the hexagonally ordered domains can originate and grow in the bulk of the membrane by acquiring nanopores from neighbouring domains and later disappear by losing all their nanopores to other domains.

Figure 2(g) shows an SEM image taken from the cross-section of the 40 μm NPA membrane, where it is possible to observe a spindle-like shape of the a typical domain, which originates, grows and disappear in the bulk of the membrane. Since nanopores gradually transit from one domain to another, such a smooth transition does not create sharp contrast on the SEM image. The grain boundaries can only be distinguished by careful examination of the deviations from straight paths of the nanopores. In order to give a guidance to the eye, there are four arrows, which show the point of origin of the domain, its maximum width and the point of fade.

One can easily catch our idea about the structure of the thick NPA membrane by imagining a bundle of long and hollow spaghettis, which were put into a tight cylinder, boiled and dried. Although every cross-section of the cylinder will show a structure of hexagonally ordered domains, there will be no straight channels due to twisting of spaghettis.

Although the effect of twisting of nanopores is detected by SANS only starting from the aspect ratio of ~1000, this means that the majority of nanopores already changed their domains during the growth. The nanopores at domain boundaries can change the direction of their growth more easily than the nanopores inside the domains, which are fixed by hexagonally ordered neighbours. Therefore some of the nanopores can have very twisted shape even from the beginning of the growth process.

When the thickness of the NPA membrane is increasing the portion of nanopores that migrated from one domain to another upon their elongation is increasing as well. As a result, the majority of nanopores is not straight anymore, which is manifested as an increase of angular misorientation of the domains and azimuthal blurring of the 2D SANS pattern. In contrast, there is no increase in radial smearing, which means that the average distance between nanopores remains constant. In order to assess angular misorientation of the domains, we fitted the intensity of the peaks $I(\phi)$ on 2D SANS patterns in the a narrow sector of $\pm 30^{o}$ around the peaks maxima (see figure 2(f)). The values of ϕ-mosaic full-width-at-half-maximum (FWHM) for the 2D SANS patterns (b), (c) and (d) of the figure 2 were 12.7, 19.3 and 23.6 degrees respectively.

The 2D SANS pattern of the thickest membrane is almost isotropic, which suggests an absence of preferential orientation among the domains. However, we should remember that 2D SANS pattern is just a superposition of scattering from 3D arrangement of individual domains that exist in the bulk of the membrane. If we slice this thick membrane into thin layers of approximately 10 μm, where nanopores are almost straight, and take their 2D SANS patterns separately then we will again get a small misorientation angle of around 10-12 degrees for each individual slice. However, the individual 2D SANS patterns of the slices will be misoriented among themselves in such a way that their superposition will give us almost isotropic 2D SANS pattern of the initial thick membrane.

We can conclude that although all nanopores pass the entire membrane from top to bottom and their average interpore distance is constant, they are not perfectly straight. This phenomenon should be taken into account

considering usage of the self-ordered nanoporous alumina membranes for the fabrication of nanodevices based on long parallel arrays of nanowires, because the twisted shape of some quantity of nanopores can affect properties of nanostructures grown inside the NPA template.

4. Conclusions

In this paper we studied the self-ordering processes in nanoporous alumina (NPA) during the initial stages of anodization as well as redistribution of nanopores between the ordered domains upon the growth of the NPA. The formation and ordering of the nanopores can be qualitatively divided into three stages: (1) nucleation of randomly distributed nanopores with broad radius distribution, (2) narrowing the radius distribution and (3) slow evolution toward ordering of pores into quasi-crystalline hexagonal lattice with ordered domains. SANS measurements of highly ordered nanoporous alumina membranes indicate the presence of orientational correlation between the domains. The compressive stress on the Al/Al_2O_3 interface, which originates from the volume expansion of aluminium oxide promotes both the hexagonal ordering of nanopores and the orientational correlation of the domains because the high misorientation angles are energetically unfavourable in such a strained environment. As a result the nanoporous structure eventually reaches a metastable configuration with a small misorientation angle between the domains. However, even after the nanoporous system reaches the highly-ordered state, the ends of growing nanopores at the Al/Al_2O_3 interface are still moving along or across the domain boundaries in order to relax local variations in the compressive stress. This process results in twisting of nanopores and manifests as azimuthal smearing of the SANS signal. The nanopores grow through the entire membrane without renucleation while the ordered domains to which they belong can be rather described as virtual entities that originate, evolve and disappear in the bulk of the membrane by dynamically acquiring and then loosing nanopores during their growth.

Acknowledgements

This research project was supported by the European Commission under the 6th Framework Programme through the Key Action: Strengthening the European Research Area, Research Infrastructures (contract no: RII3-CT-2003-505925), by the Grant-in Aid for Scientific Research of Ministry of Education, Culture, Sports, Science and Technology of Japan and by New Energy Development Organization (NEDO) of Japan.

References

1. Thompson G E and Wood G C 1981 *Nature* 290 230.
2. Mei X, Blumin M, Kim D, Wu Z and Ruda H E 2003 *J. Cryst. Growth* 251 253.
3. Shimizu T, Xie T, Nishikawa J, Shingubara S, Senz S and Gosele U 2007 *Adv. Mater.* 19 917.
4. Riveros G, Green S, Cortes A, Gomez H, Marotti R E and Dalchiele E A 2006 *Nanotechnology* 17 561.
5. Che G, Lakshmi B B, Fisher E R and Martin C R 1998 *Nature* 393 346.
6. Turkevych I, Pihosh Y, Goto M, Kasahara A, Tosa M, Kato S, Takehana K, Takamasu T, Kido G and Koguchi N 2008 *Thin Solid Films* 516 2387.
7. Wang B 2007 *Nanotechnology* 18 365601.
8. Lee W, Ji R, Gosele U and Nielsch K 2006 *Nature Materials* 5 741.
9. Nielsch K, Choi J, Schwirn K, Wehrspohn R B and Gosele U 2002 *Nano Letters* 2 677.
10. Nielsch K, Muller F, Li A P and Gosele U 2000 *Adv. Mater.* 12 582.
11. Allen A J 2005 *J. Amer. Ceram. Soc.* 88 1367.
12. Kulda J and Mikula P 1983 *J. Appl. Cryst.* 16 498.
13. Strunz P, Saroun J, Mikula P, Lukas P and Eichhorn F. 1997 *J. Appl. Cryst.* 30 844.
14. Ryukhtin V and Saroun J 2002 *Appl. Phys.* A 74 S1158.
15. Ryukhtin V, Saroun J, Harjo S, Motohashi Y, Baron M and Loidl R 2003 *J. Appl. Cryst.* 36 478.
16. Oster G and Riley D P 1952 *Acta Cryst.* 5 272.
17. Jones A F, Parker I B and Stacey M H 1991 *J. Appl. Cryst.* 24 607.
18. Marchal D, Bourdillon C and Deme B 2001 *Langmuir* 17 8313.
19. Marchal D and Deme B 2003 *J. Appl. Cryst.* 36 713.
20. Marchal D and Deme B 2005 *Eur. Biophys. J.* 34 170.
21. Grigor'ev S V, Grigor'eva N A, Syromyatnikov A V, Napol'skii K S, Eliseev A A, Lukashin A V, Tret'yakov Y D and Eckerlebe H 2007 *JETP Letters* 85 449.
22. Masuda H and Fukuda K 1995 *Science* 268 1466.
23. Boyer D and Vinals J 2002 *Phys. Rev. Lett.* 89 055501-1.